Fuel 416 (2026) 138473

Contents lists available at ScienceDirect

Fuel

journal homepage: www.elsevier.com/locate/jfue

Full length article

Conversion of suspension fuel droplets in the flame zone of an entrained flow gasifier

Manuel Haas[a,*], Sabine Fleck[a], Frederik Scheiff[a,b], Thomas Kolb[a,b]

[a] Karlsruhe Institute of Technology (KIT), Institute for Technical Chemistry, Gasification Technology (ITC vgt), Herrmann-von-Helmholtz-Platz 1, 76344 Eggenstein-Leopoldshafen, Germany

[b] Karlsruhe Institute of Technology (KIT), Engler-Bunte-Institute, Fuel Technology (EBI ceb), Engler-Bunte-Ring 1, 76131 Karlsruhe, Germany

HIGHLIGHTS

- Flame structure of liquid and suspension fuel compared in an Entrained Flow Gasifier.
- 2-Phase Free Jet Model expanded to suspension fuels and validated by OH-LIF.
- Experiment shows 72% longer flame with analog structure for suspension fuel.
- Flame length mostly determined by spray parameters in investigated case.
- Comparison of 3 droplet models showed strong differences in prediction of flame.

ARTICLE INFO

Keywords:
Entrained flow gasification
Inverse diffusion flame
Spray
Free jet
Suspension
Carbon cycle
Syngas

ABSTRACT

The High-pressure Entrained Flow Gasification (EFG) process can play an important role in future production chains with a closed carbon cycle because of its ability to generate a high-quality syngas from waste-based fuels, e.g., pyrolysis oils and suspensions derived from biomass and mixed plastic wastes. This work aims to improve the understanding of the conversion processes in the EFG flame zone for suspension fuels by applying a well-defined model suspension (monoethylene glycol and beech-wood char) in a combined experimental and numerical approach. A 2-Phase Free Jet Model is used to numerically investigate the reacting fuel spray and to perform a sensitivity study on suspension droplet conversion models. Modeled flame structures are validated by OH-LIF experiments at an atmospheric EFG. Results show that the flame structure for the suspension fuel is mainly determined by entrainment of syngas into the oxidizer jet and liquid fuel evaporation, whereas solid reactions are shown to play a minor role. Different suspension droplet conversion models are compared in a sensitivity study, showing a strong impact of the modeling approach on the amount of liquid fuel evaporation, which in turn influences flame structure. The insights of the study serve as a valuable basis for further research elucidating the coupled transport and reaction phenomena in the EFG flame, in particular the formation and conversion of intermediate solid products.

1. Introduction

1.1. Motivation and objectives

Entrained Flow Gasification (EFG) is a process to convert organic feedstocks to syngas, which is a valuable intermediate product used for the production of base chemicals. Today, the Entrained Flow Gasification (EFG) process is predominantly used to convert fossil based fuels into syngas. In order to enable a transition towards a circular economy with a closed carbon cycle, fossil based feedstocks need to be replaced by biogenic and anthropogenic residues. Typical waste based feedstocks to be applied for EFG in circular process chains are eg. oils, chars and their suspensions originating from pyrolysis of mixed wastes or biomass. These materials are typically of low fuel quality and are characterized by highly variable compositions, high heterogeneity and high amounts of inorganic impurities [1–5], requiring a fuel flexible process.

In EFG systems, the processes in the burner near field determine temperature field and fuel conversion and are thus critical for process efficiency. Even though suspension fuels have already been applied for

* Corresponding author.
Email address: manuel.haas@kit.edu (M. Haas).

https://doi.org/10.1016/j.fuel.2026.138473
Received 30 September 2025; Received in revised form 9 January 2026; Accepted 18 January 2026
Available online 29 January 2026

Nomenclature

Symbol	Definition
A_{gas}	Nozzle gas exit area
$c_{p,gas}$	Heat capacity of gas phase
$c_{p,liq}$	Heat capacity of liquid phase
$c_{p,sol}$	Heat capacity of solid phase
d	Droplet diameter
$d_{eq}d_{eq}$	Equivalent nozzle diameter
d_0	Initial droplet diameter
$d_{sol,0}$	Initial solid particle diameter
$d_{32,sol}$	Sauter mean diameter of solid particles
$\Delta h_{vap,liq}$	Mass specific enthalpy of evaporation
$\Delta h_{R,i}$	Mass specific reaction enthalpy
δ_c	Critical layer thickness
$E_{A,i}$	Activation energy of gasification reaction with component i
$E_{A,vol}$	Activation energy of devolatilization reaction
ϵ_{rad}	Emissivity factor
$\epsilon_{por,c}$	Critical porosity of solid packing
η_i	Effectiveness factor for reaction i
η_{liq}	Liquid viscosity
$\dot{H}_{reac,drop}$	Reaction and phase change enthalpy flow of droplet
h_{GA}	Mass specific enthalpy of gasification agent
h_{SG}	Mass specific enthalpy of syngas
ID_{32}	Integral Sauter mean diameter of spray
J_{gas}	Gas momentum flow
K	Evaporation parameter
$k_{0,vol}$	Pre-exponential factor of devolatilization reaction
$k_{0,i}$	Pre-exponential factor of gasification reaction with component i
L_{OH}	Longitudinal extension of OH zone
λ_{abs}	Gas phase absolute stoichiometry
λ_{gas}	Gas phase thermal conductivity
M_C	Molar mass of carbon
$m_{liq,drop}$	Mass of liquid phase in droplet
$m_{sol,drop}$	Mass of solid phase in droplet
$m_{sol,drop,vol}$	Mass of volatiles in droplet
$m_{sol,drop,fix}$	Mass of fixed carbon in droplet
$\dot{m}_{fuel}$	Fuel mass flow fed to reactor
$\dot{m}_{FG}$	Mass of converted solid fuel in jet
$\dot{m}_{FV}$	Mass of fuel vapor in jet
$\dot{m}_{GA}$	Mass of gasification agent in jet
$\dot{m}_{SG}$	Mass of syngas in jet
$\dot{q}_{con}$	Convective heat flow to droplet collective
Q_3	Volume weighted particle size distribution
$\dot{Q}_{con,drop}$	Convective heat flow to single droplet
$\dot{Q}_{rad,drop}$	Radiative heat flow to single droplet
r_i	Intrinsic solid reaction rate
ρ_{liq}	Liquid density
t	Time
T_{ad}	Adiabatic reaction temperature
T_{drop}	Droplet temperature
T_∞	Bulk temperature
$\theta_{0.9}$	Spray angle
$u_{GA,0}$	Gas exit velocity at nozzle
$\dot{V}_{GA}$	Volume flow (NTP) of gasification agent fed to reactor
V_{OH}	Volume of OH zone
$x_{sol,0}$	Initial solid mass fraction in suspension
$X_{liq,drop}$	Evaporated fraction of liquid from a Suspension droplet
$X_{sol,drop}$	Solid conversion of a Suspension droplet
$X_{sol,dry,OH}$	Mass fraction of dried solid phase within OH zone
$X_{liq,OH}$	Evaporated liquid mass fraction within OH zone
$X_{sol,OH}$	Converted solid mass fraction within OH zone
x_i	Mixture fraction of component i
x_{FG}	Mass fraction of converted solid fuel in jet
x_{FV}	Mass fraction of fuel vapor in jet
x_{GA}	Mass fraction of gasification agent in jet
x_{SG}	Mass fraction of syngas in jet
$y_{O2,GA}$	Oxygen volume fraction in gasification agent

example for coal-water-slurry at industrial level [6–10] and for biogenic pyrolysis slurry at pilot scale [1], the conversion processes of suspension fuels in the EFG flame zone have not been sufficiently studied in literature. During the conversion of suspension droplets, the physical properties of liquid and solid phases, heating rate, surrounding atmosphere as well as the chemical reactions between the components in the droplet determine the resulting histories of droplet mass, composition and morphology [11–15]. This influences the release rate of fuel vapor and volatiles to the gas phase, which can impact local stoichiometry in the EFG flame and thus affect flame geometry and temperature field [16,17]. The morphology and composition of the remaining solid particles determine their further conversion downstream of the flame in the EFG reactor and are thus relevant for global fuel conversion.

As outlined below (see Section 1.2), most studies in literature apply simplified droplet models and do not assess suspension droplet conversion in the flame zone in detail, posing a major research gap. Additionally, the differences between liquid and suspension fuel EFG flames have not been systematically investigated. To enable an efficient and fuel flexible operation of EFG reactors for waste based suspension feedstocks, a more detailed understanding of these aspects is thus necessary.

The scope of this work is to investigate the sub-processes during the conversion of suspension fuel droplets in an EFG flame using a well-defined reference fuel (MEG w/ beech wood char). A 2-Phase Free-Jet model is expanded from liquid to suspension fuels and validated by experiments in an atmospheric entrained flow gasifier. The model is used to study the conversion of suspension droplets in the EFG flame and to systematically compare selected suspension droplet models. Parts of this work have been presented in [18] and are replicated with modifications. Additional experimental data and information on feedstocks are provided in the supplementary material.

1.2. Modeling approaches for suspension fuel droplet conversion

During conversion in the EFG flame zone, suspension droplets experience high temperatures and heating rates in both oxidizing and reducing atmospheres [7,16], leading to a multitude of complex phenomena. When a suspension droplet is heated up, rising liquid vapor pressure leads to the onset of evaporation. Liquid fuel is transferred to the gas phase while solid particles remain in the droplet. Accumulation and caking of solid particles at the droplet surface [19,20] and secondary pyrolysis of less volatile liquid fuel components [5,21] can then lead to the formation of a solid shell at the droplet surface. These processes are especially relevant at high heating rates typical for the flame zone in EFG systems. Shell formation processes can inhibit liquid evaporation, resulting in liquid evaporation times that can be significantly longer than those for pure liquid droplets [22–24]. The presence of a solid phase at the droplet surface can on the other hand initiate local boiling and pyrolysis inside the droplet, leading to gas formation and pressure increases that can result in swelling or fragmentation of the droplet [13,14,25,26]. These processes can cause a wide range of possible droplet conversion histories, which are further detailed in literature [11]. Remaining solid

Table 1
Comparison of applied droplet models.

Aspect	Wet Particle	Fragmenting Particle	Shell Formation
Droplet description	Single solid particle surrounded by liquid film.	Solid particles always homogeneously distributed in liquid phase, breakup into single particles surrounded by liquid film.	Solid particles initially homogeneously distributed in liquid phase, shell formation by enrichment of solid particles at droplet surface.
Droplet size	Determined by solid particle diameter.	Independent from solid particle diameter.	Independent from solid particle diameter.
Solid particles	Single particle	Single particle	Agglomerate of multiple particles (hollow sphere)
Evaporation stages	1	2	2
Stage transition	-	Solid particle packing reaches $\epsilon_{\mathrm{por,c}} = 0.476$	Shell thickness reaches $\delta_c = 3d_{\mathrm{p}}$
$\frac{\mathrm{d}m_{\mathrm{liq,drop}}}{\mathrm{d}t} =$	$-\pi d^2 \cdot \alpha \cdot \frac{\ln\left(1+c_{\mathrm{p,gas}} \cdot \frac{(T_\infty - T_{\mathrm{drop}})}{\Delta h_{\mathrm{vap,liq}}}\right)}{c_{\mathrm{p,gas}}}$	$-\pi d^2 \cdot \alpha \cdot \frac{\ln\left(1+c_{\mathrm{p,gas}} \cdot \frac{(T_\infty - T_{\mathrm{drop}})}{\Delta h_{\mathrm{vap,liq}}}\right)}{c_{\mathrm{p,gas}}}$	$-\frac{\pi \cdot d \cdot 2 \cdot \lambda_{\mathrm{gas}}}{c_{\mathrm{p,gas}}} \cdot \ln\left(1 + c_{\mathrm{p,gas}} \cdot \frac{(T_\infty - T_{\mathrm{drop}})}{\Delta h_{\mathrm{vap,liq}}}\right)$

particles and agglomerates are further converted in heterogeneous gas-solid reactions, which typically take place on longer time scales than the initial conversion steps. The reactions of these structures are influenced by their morphology, which is strongly affected by the previous conversion steps [14,15].

CFD simulation studies of EFG reactors fed by suspension fuels usually pay little attention to describing the slurry droplet behavior in reactor simulations, as the detailed description of a large number of suspension fuel droplets causes high computational cost [27]. Most studies in literature thus apply simple suspension droplet models in order to neglect the sub-processes during suspension droplet conversion. A systematic comparison of different droplet conversion model approaches for suspension fuels and their impact on the processes in the EFG flame zone has not been conducted to the author's knowledge. In the following, a brief overview of suspension droplet modeling approaches applied in EFG literature is given:

- The simplest approach applied in modeling suspension gasification is to inject the liquid phase as pure liquid droplets separate from the solid particles in order to avoid using a suspension droplet model [28–30].
- The overwhelming majority of published work on simulation of suspension fuel fed EFG uses a Wet Particle approach [9,10,31–38]. This simplified approach assumes a spherical solid core which is surrounded by a liquid film. Common liquid droplet evaporation models can be applied until the liquid fraction is completely evaporated. Because this is the most widely used approach in EFG simulations, it was implemented in this work with further details given in Section 2.1.3.
- Another approach for simulation of an EFG system applies a standard liquid evaporation model while assuming a simultaneous release of char with liquid during the evaporation process. [27,39] .

More complex suspension droplet models considering additional effects are also reported in literature. Several model approaches were developed to account for one or more of the above discussed processes. To the author's best knowledge, none of these models have been applied in published works on EFG systems.

- Different models describe the formation of a solid shell at the droplet surface [11,19,20,40], leading to a hollow solid agglomerate (cenosphere). The occurrence of such agglomerates has been documented for EFG conditions in literature [41,42]. The model developed by Lee and Law [40] is chosen as an example of a simple cenosphere formation model in this work (see Section 2.1.5).
- Another category of suspension droplet models uses a wet kernel approach, which assumes the suspension droplet diameter decreases during liquid evaporation until a compact agglomerate of solid particles is formed. During the drying of this agglomerate, liquid evaporation is inhibited by the mass transport through the porous structure.[13] These models typically involve radial temperature gradients and require a discretization of the particle [19,43–46]. Some models also take pressure rise in the agglomerate leading to fragmentation into account [13]. A simplified version of this approach is implemented in Section 2.1.4.
- More complex models have been developed to include the pyrolysis of the liquid phase, requiring a discretized calculation of heat and mass transport in the particle together with a model of the pyrolysis reactions specific to the fuel and process conditions [47–49].

2. Methods

2.1. Two-phase Free Jet Model (2-Ph-FJM)

A 2-phase Free-Jet Model (2-Ph-FJM) is applied in this work to investigate the conversion of suspension droplets in the EFG flame zone. The model was expanded in order to account for the conversion of suspension fuel droplets and the reactions of the solid phase remaining after evaporation. The modifications to the 2-Ph-FJM are detailed in [18] and are summarized in the following sections. The original model basis is described in Section 2.1.1, followed by a description of the implementation of suspension droplets into the 2-Ph-FJM (Section 2.1.2). Conversion of suspension droplets is described using the models in Sections 2.1.3 – 2.1.5, which are taken as examples of the different approaches outlined in the introduction (Section 1.2). The droplet models are summarized in Table 1. The conversion of the remaining solid phase is described according to Section 2.1.6.

2.1.1. Model basis

The 2-Ph-FJM is a semi-empirical model that describes mixing and flow field of a free jet consisting of gasification medium and fuel spray emerging into a quiescent hot syngas atmosphere on the basis of turbulent free jet theory. The model was originally developed by Hotz [50] and further extended and validated by Haas [16,18]. In order to describe the effect of the liquid phase on turbulent gas phase mixing in the 2-Ph-FJM, single phase free jet equations were modified by applying coefficients for turbulent exchange that were empirically determined for two phase jets [50].

In the model, the gas jet emerges into the model geometry through a circular orifice with an equivalent diameter d_{eq}, which serves as a scaling parameter for turbulent jet mixing:

$$d_{\mathrm{eq}} = \sqrt{\frac{4 \cdot A_{\mathrm{gas}}}{\pi}}. \tag{1}$$

A_{gas} corresponds to the gas exit area of the burner nozzle. The jet medium mixes with the surrounding syngas, which is assumed to have the equilibrium composition of the input streams at the reactor temperature of 1200 °C. The liquid phase is injected into radially discretized segments at the nozzle outlet, representing fixed droplet trajectories. In each radial segment, a droplet collective of 50 equally spaced droplet size classes based on Weibull Q_3-distributions derived from the experimental input data is injected. Details on the liquid injection are given in prior works [16].

Gas and liquid phases are coupled through balances of mass, momentum and energy. Droplets are accelerated along fixed trajectories originating at the nozzle exit by solving a momentum balance between gas and liquid phases using Reynolds number dependent coefficients of drag. Heat transfer from the gas phase leads to droplet heating and evaporation, resulting in transfer of fuel vapor to the gas phase. In the original model, these processes are described using the d^2-law for droplet evaporation [50].

Chemical equilibrium is assumed for the gas phase mixture consisting of gasification medium, syngas and fuel vapor. Apart from the core region in the jet, mean gas temperatures are above 1200 °C and can exceed 2000 °C in the flame front. Under these conditions, oxidation reaction rates defining the flame structure exceed turbulent mixing rates, justifying the assumption of chemical equilibrium as an approximation. Gas phase equilibrium temperature and species concentrations are calculated using a Gibbs Free Energy minimization approach. As equilibrium species, the main species O_2, N_2, CO_2, CO, H_2 and H_2O are considered together with the secondary components OH, O, H and NO. Formation of by-products like CH4 and soot typically occurs on longer time scales and cannot be predicted by this approach. These species are therefore excluded from the calculation. An investigation of reaction time scales under similar conditions is for example provided by Hunger et al. [51]. Further detail on the reaction model is given in [18].

2.1.2. Suspension droplets in the 2-Ph-FJM

This section describes the modifications implemented in the 2-Ph-FJM in order to describe the conversion of suspension fuels [18]. As in the original model, suspension droplets are injected at the nozzle exit according to predefined droplet size and mass flux distributions. Each droplet in the model contains the same initial mass fraction of solid $x_{sol,0}$. Solid particles in the droplets all feature the same initial diameter which corresponds to the Sauter Mean Diameter of the applied beech-wood char $d_{32,sol}$.

Momentum transfer between gas phase and droplets is calculated identically to the original model. The energy balance for each suspension droplet and solid particle is now given by

$$(m_{sol,drop} \cdot c_{p,sol} + m_{liq,drop} \cdot c_{p,liq}) \cdot \frac{dT_{drop}}{dt} = \dot{Q}_{con,drop} + \dot{Q}_{rad,drop} + \dot{H}_{reac,drop} \quad (2)$$

The solid and liquid mass in the suspension droplet are given by $m_{sol,drop}$ and $m_{liq,drop}$ with their respective heat capacities $c_{p,sol}$ and $c_{p,liq}$. The energy balance considers convective and conductive heat transfer $\dot{Q}_{con,drop}$, radiative heat transfer $\dot{Q}_{rad,drop}$ and the change of thermal energy induced by reaction and phase change $\dot{H}_{reac,drop}$. Convective heat transfer is calculated using a Nusselt correlation. Radiative heat transfer is calculated assuming a droplet emission factor $\epsilon_{rad} = 1$ and a radiation temperature of 1200°C, corresponding to the reactor wall. The term $\dot{H}_{reac,drop}$ in Eq. (2) is during evaporation expressed by the mass specific heat of evaporation $\Delta h_{vap,liq}$ and during solid conversion by the heat of the Boudouard and heterogeneous water gas reactions $\Delta h_{R,CO2}$ and $\Delta h_{R,H2O}$ and their reaction rates r_i (also see Section 2.1.6):

$$\dot{H}_{reac,drop} = \frac{dm_{liq,drop}}{dt} \cdot \Delta h_{vap,liq} + \frac{dm_{sol,drop}}{dt} \cdot \left(\frac{r_{CO2}}{r_{CO2} + r_{H2O}} \Delta h_{R,CO2} + \frac{r_{H2O}}{r_{CO2} + r_{H2O}} \Delta h_{R,H2O} \right) \quad (3)$$

The rates of mass loss for liquid and solid phases are given by the respective evaporation and char conversion models (see sections below).

For description of the gas phase, the original 2-Ph-FJM uses a local ternary mixture fraction of the mass flows of jet medium $\dot{m}_{GA}$, surrounding syngas $\dot{m}_{SG}$ and fuel vapor $\dot{m}_{FV}$, which was calculated based on the free jet equations and droplet evaporation to describe the gas phase [50]. In order to account for the conversion of suspension fuels, the local mixing ratio is now expanded to additionally contain the fuel mass flow $\dot{m}_{FG}$ that enters the gas phase through solid fuel gasification and devolatilization reactions. The local mixing ratio for stream i is thus given in each cell by

$$x_i = \frac{\dot{m}_i}{\dot{m}_{GA} + m_{SG} + \dot{m}_{FV} + \dot{m}_{FG}}. \quad (4)$$

The recirculation gas in the model calculations was assumed to have the equilibrium gas phase composition of the input streams with the MEG fully converted and a char conversion degree of 100%. A sensitivity study on this parameter is provided based on gas phase balancing of the experimental points at the REGA gasifier (see supplementary material Appendix A4 and Appendix A6). Recirculation of solid particles into the flame is not taken into account in the model. In the following, gas phase composition and temperature are calculated using the Gibbs-reactor equilibrium approach described above. The gas phase enthalpy necessary for the calculation is therefore expanded by stream FG:

$$h_{gas} = x_{GA} \cdot h_{GA} + x_{SG} \cdot h_{SG} - \dot{q}_{con} + x_{FV} \cdot h_{liq} + x_{FG} \cdot h_{sol}. \quad (5)$$

using the heats for the gas streams h_{GA}, h_{SG} given at their respective temperatures by NASA polynomials [52], for liquid $\Delta h_{f,liq}$ by tabulated values [53] and for solid $\Delta h_{f,char}$ derived from the char heating value. The heat transfer to the liquid phase is considered by $\dot{q}_{con}$. The calculation of the gas phase temperature and composition alters the conditions for droplet evaporation and solid conversion. The calculation of droplet conversion and gas phase are thus repeated in an iterative approach.

For evaluation of the flame structures, the OH distribution is used. The longitudinal extension of the OH zone L_{OH} is applied as a characteristic parameter of the flames and is defined as the axial nozzle distance at which the OH concentration falls below 10% of its maximum value. The OH volume V_{OH} is accordingly defined as the volume within the 10% OH contour. The OH contour is also used to define fuel conversion progress variables for the flame. The liquid conversion progress within the OH volume $X_{liq,OH}$ is defined by the total mass of evaporated liquid within the 10% OH contour integrated over all trajectories and droplet size classes. The solid conversion within the OH zone $X_{sol,OH}$ is defined analogously. The drying conversion $X_{sol,dry,OH}$ considers solid mass that has completely dried and is available for reaction with the gas phase. In order to assess the degree of oxidation in the gas phase, the absolute stoichiometry is defined as

$$\lambda_{abs} = \frac{N_O}{2 \cdot N_C + 0.5 \cdot N_H} \quad (6)$$

with the numbers of oxygen, carbon and hydrogen atoms N_O, N_C and N_H. [18]

2.1.3. Suspension droplet model 1: wet particle

The wet particle approach is the most widely applied droplet model for simulation of gasification systems (see Section 1.2). The model assumes the droplet is one solid particle surrounded by a liquid film. The initial diameter of the droplet in this description is thus determined by the diameter of the solid particle and the corresponding volume of the liquid phase and does not allow for defining a droplet size distribution.

The droplet is first heated according to Eq. (2). Evaporation during the heat-up phase is calculated using a mass transfer limited approach using the liquid vapor pressure at the droplet surface and a Sherwood correlation [31,32]. When the liquid boiling point is reached, a quasi steady state model in form of a Spalding-type evaporation rate is applied: [31,32]

$$\frac{dm_{liq,drop}}{dt} = -\pi d^2 \cdot \alpha \cdot \frac{\ln\left(1 + c_{p,gas} \cdot \frac{(T_\infty - T_{drop})}{\Delta h_{vap,liq}}\right)}{c_{p,gas}} \quad (7)$$

with T_∞ being the bulk gas temperature and $c_{p,gas}$ the specific heat capacity of the surrounding gas atmosphere. After complete evaporation of the liquid fuel, the remaining solid core is regarded as one single particle that reacts according to the description in Section 2.1.6 [18].

2.1.4. Suspension droplet model 2: fragmenting particle model

This model is based on the wet-kernel models (Section 1.2). The model applies a size distribution of suspension droplets that contain a number of solid particles defined by $x_{sol,0}$ featuring an initial solid particle diameter $d_{sol,0}$. The model assumes fast mixing within a suspension droplet, leading to uniformly distributed solid particles in the liquid phase.

In the first evaporation phase, the droplet heating and liquid evaporation rate are again described by Eqs. (2) and (7). During the evaporation process, the solid volume fraction in the droplet increases, until a critical volume fraction is reached where the particles can no longer contract. This value is assumed to correspond to the porosity of a cubical packing of spheres ($\epsilon_{por,c} = 0.476$). The model does not account for the formation of a solid agglomerate. This is the case when solid particles do not exhibit caking behavior under high temperatures, and pyrolysis reactions in the liquid phase are negligible. Instead, after reaching $\epsilon_{por,c}$, a droplet microexplosion is assumed in which the suspension droplet disintegrates into its individual solid particles each surrounded by a liquid film corresponding to the remaining liquid in the droplet. These wet char particles are then converted according to the Wet Particle model (Section 2.1.3) [18].

2.1.5. Suspension droplet model 3: shell formation model

The droplet model developed by Lee and Law [40] predicts liquid evaporation rate and shell formation for suspension droplets in two steps. The model applies a size distribution of suspension droplets that contain a number of solid particles defined by $x_{sol,0}$ featuring an initial solid particle diameter $d_{sol,0}$. At the start of the evaporation process, the droplet is assumed to have a spatially homogeneous distribution of solid particles suspended in the liquid phase. In contrast to the Fragmenting Particle model, the transport of solid particles in the droplet is slow in comparison to the liquid evaporation time.

Particle heat up to the liquid boiling point is modeled using Eq. (2) assuming a homogeneous temperature distribution in the particle. Liquid evaporation during the heat up phase is not taken into account by the model. After reaching the liquid boiling point, liquid evaporation is described using the d^2-law

$$d^2(t) = d_0^2 - K \cdot t. \tag{8}$$

using the droplet diameter d and

$$K = \frac{8 \cdot \lambda_{gas}}{\rho_{liq} \cdot c_{p,gas}} \cdot \ln\left(1 + c_{p,gas} \cdot \frac{(T_\infty - T_{drop})}{\Delta h_{vap,liq}}\right). \tag{9}$$

The liquid density is expressed by ρ_{liq} and the gas phase heat conductivity is expressed by λ_{gas}. The liquid mass loss rate during this process is given by

$$\frac{dm_{liq,drop}}{dt} = -\frac{\pi}{4} \cdot d \cdot \rho_{liq} \cdot K. \tag{10}$$

During the liquid evaporation process, solid particles accumulate at the droplet surface due to the receding evaporation front and the lack of particle transport in the liquid phase. Solid particles therefore densify at the droplet surface until a critical porosity ϵ_c defined by a cubic packing of spheres is reached. After reaching a critical layer thickness δ_c of solid particles, a rigid porous shell is established. At this point, the evaporation process switches to a fixed diameter stage [40].

During this second stage, the mass flow of evaporating liquid is again given by Eq. (10) using the droplet diameter defined by the rigid shell. Inhibition of mass transport through the porous shell is not taken into account. In the model, the continuous depletion of liquid through evaporation creates a spherical expanding space of vapor within the droplet. The thickness of the porous shell further increases through continuous deposition of solid particles on its inside. When the liquid is completely evaporated, a solid agglomerate in form of a hollow sphere with a shell thickness calculated by a solid mass balance is left [18].

2.1.6. Char reactions

When the liquid evaporation process described by the models in Sections 2.1.3 - 2.1.5 is complete, solid particle conversion is modeled using devolatilization reactions and heterogeneous gasification reactions [18]. The total solid mass $m_{sol,drop}$ is separated into a volatile mass $m_{sol,drop,vol}$ and a fixed carbon mass $m_{sol,drop,fix}$ which has been determined in literature for the used char [54].

$$m_{sol,drop} = m_{sol,drop,vol} + m_{sol,drop,fix} \tag{11}$$

The individual particles are modeled to have a spatially uniform temperature distribution. The Uniform Conversion Model (UCM) is applied, i.e., the depletion of mass due to devolatilization and heterogeneous reactions is assumed to only affect particle density, resulting in a constant solid particle diameter throughout its entire conversion.

Devolatilization of the char is modeled using a single first order Arrhenius law approach, utilizing kinetic data determined for the applied char in a Drop-Tube Reactor (DTR) [54]:

$$\frac{dm_{sol,vol,drop}}{dt} = -m_{sol,vol,drop} \cdot k_{0,vol} \cdot exp\left(-\frac{E_{A,vol}}{RT}\right) \tag{12}$$

with the universal gas constant R, the pre-exponential factor $k_{0,\,vol}$ and activation energy $E_{A,vol}$ for the devolatilization reaction. The heterogeneous char reactions with CO_2 and H_2O are described by

$$\frac{dm_{sol,drop,fix}}{dt} = -m_{sol,drop,fix} \cdot \bar{M}_C \cdot (r_{CO2} \cdot \eta_{CO2} + r_{H2O} \cdot \eta_{H2O}) \tag{13}$$

with the molar mass of carbon $\bar{M}_C$ and the intrinsic reaction rate r_i. The effectiveness factor η is included to account for pore diffusion limitations that are relevant under gasification conditions [6,55] and is calculated using a Thiele-modulus ϕ [7]. The intrinsic reaction rates were described using a power law approach

$$r_i = k_{0,i} \cdot exp\left(-\frac{E_{A,i}}{RT}\right) \cdot p_i^{n_i} \tag{14}$$

with the partial pressure p_i and the reaction order n_i for the component i (CO_2, H_2O). The kinetic data for the used char were determined in a Pressurized Single Particle Reactor (pSPR) for both reactants [56].

2.2. Gasification experiments

The gasification experiments were carried out at the Research Entrained Flow Gasifier (REGA), which has been described in previous publications [16,57]. The gasifier consists of a ceramic tube with an inner diameter of 0.28 m and a length of 3.0 m. Reactor walls are electrically heated to a temperature of 1200 °C. The reactor is equipped with nitrogen purged quartz-glass windows to enable optical access and features an axially movable burner. The gasifier is operated under atmospheric pressure using oxygen enriched air as gasification medium. Pure monoethylene glycol (MEG) and a suspension of 70 wt-% MEG with 30 wt-% beech wood char (BWC) were applied as fuel. The Sauter mean diameter of the char particles was determined to be $d_{32,sol} = 9$ µm. For further details on the char and its properties see supplementary material Appendix A.1. The gasifier operating conditions for MEG and suspension fuel are given in Table 2. Both experimental conditions were designed to have identical gas input volume flows of $\dot{V}_{GA} = 7,5 m^3/h$ to achieve equal jet mixing in the burner near region while modulating oxygen content in the gasification agent $y_{O2,GA}$ to give an adiabatic equilibrium temperature of 1700 °C for all setpoints.

For fuel feeding, an external mixing burner nozzle was applied. The liquid fuel is fed as a central jet while the gasification medium enters the reactor through a surrounding annulus with a nozzle equivalent diameter of $d_{eq} = 5.0$ mm resulting in an outlet gas velocity of $u_{GA,0} = 116$ m/s.

For assessment of the flame zone, an OH-LIF system and the respective measurement and post processing procedures described in former

Table 2
Operating conditions for the experimental cases.

Fuel	$x_{sol,0}$ –	$\dot{m}_{fuel}$ kg/h	$\dot{V}_{GA}$ m³/h	J_{gas} kg/m/s²	T_{ad} °C	$y_{O2,GA}$ –
MEG	0	12.4	7.5	0.34	1700	69.3
MEG + BWC	30	12.7	7.5	0.34	1700	77.3

Table 3
Viscosities and spray parameters for the experimental cases determined in the ambient spray characterization experiments.

Fuel	$x_{sol,0}$ %	η_{liq} mPas	ID_{32} μm	$\theta_{0.9}$ °
MEG	0	21	114	27
MEG + BWC	30	211	189	29

works were applied [16]. For all experimental cases, fluorescence of the OH radical was measured upon excitation at the $Q_1(8)$-line at a laser wavelength of 283.55 nm. Because the optical windows allow access to only a part of the flame, the burner was axially moved in 20 mm steps during the OH-LIF measurements. 500 images for OH fluorescence, background and offline fluorescence were taken at each measurement position during an experiment. After post-processing, the individual sections were axially appended to create an image of the entire flame zone. The experimental values for the longitudinal extension of the OH zone L_{OH} and the OH volume V_{OH} are defined based on the LIF measurements in analogy to the model calculations.

In order to interpret the experimental results and to provide input data for the model, additional droplet size and spray angle measurements were performed under ambient conditions using shadowgraphy and a mechanical patternator (see supplementary material Appendix A.2).

Particle extraction experiments were conducted in order to determine particle conversion and structure of the remaining unconverted char. The experimental procedures and results are provided in the supplementary material Appendix A.3.

3. Results and discussion

In the first part of this work (Section 3.1), the differences in flame structure between the applied liquid and suspension fuels under EFG conditions are discussed using experimental data and model calculations. The model is then used to investigate the conversion of suspension droplets in the EFG flame using different model approaches (Section 3.2). The interaction of droplet conversion and gas phase processes in the flame zone and the consequences for flame structure and fuel conversion progress are then analyzed in Section 3.3. Parts of the results in this chapter have previously been presented in [18].

3.1. Comparison of flame structure for liquid and suspension fuel

Spray parameters measured under ambient conditions for both pure MEG and the suspension fuel are given in Table 3. The addition of solid particles to the liquid phase leads to a significant increase in viscosity. This results in a larger droplet size which is reflected by the increased ID_{32}. The spray angle is only moderately widened with higher particle content, as indicated by the nearly constant values of $\theta_{0.9}$.

Fig. 1 shows results of the OH-LIF measurement for both experimental cases. The flame structure in an EFG reactor applying a central liquid jet burner can be described as a two-phase jet of oxygen rich gasification agent and fuel spray, which emerges into a hot syngas atmosphere. At the nozzle outlet, a core zone exists which is characterized by low temperatures and the absence of chemical reactions. At the boundaries of the gas jet, mixing of oxidizer and hot syngas causes exothermic oxidation reactions resulting in high temperatures and the formation of OH. Further

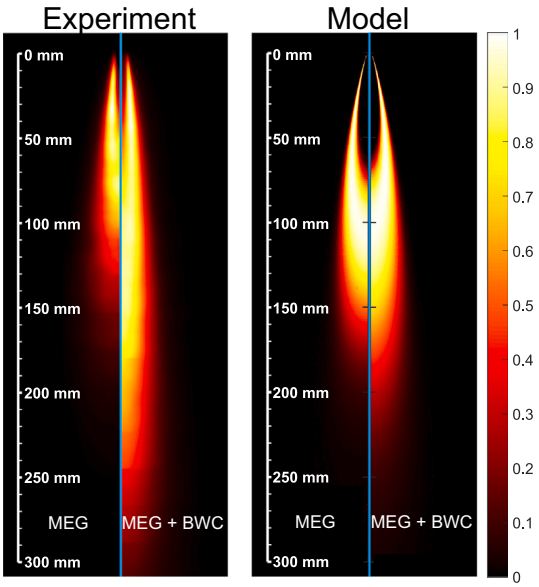

Fig. 1. Experimental OH-LIF intensities and calculated OH concentrations for cases MEG and MEG + BWC using the 2-Ph-FJM and the Fragmenting Particle model. For comparison, the fields of OH-LIF intensity and calculated OH concentration are normalized to their maximum values [18].

entrainment of syngas into the jet leads to an expansion of this high temperature oxidation zone towards the jet centerline. The oxygen in the jet medium is consumed mainly by reaction with entrained syngas and to a lesser extent by reaction with fuel vapor (see Section 3.3). Further downstream, oxygen is completely consumed and sub-stoichiometric conditions with $\lambda_{abs} < 1$ are present. Further entrainment of syngas colder than the flame temperature combined with continuing fuel evaporation leads to a decrease in temperature and OH concentration with increasing nozzle distance. Further details on this flame structure are given in literature [16,17,50].

The principal structure of the reaction zones is similar for both cases and is not altered by the presence of char particles in the suspension fuel case, as the data show. However, the OH zone for case S30-A shows a longer longitudinal extension (L_{OH} = 300 mm) in comparison to the MEG case (L_{OH} = 174 mm) in the experiment. To investigate this effect, the 2-Ph-FJM is applied. Spray data given in Table 3 were used as input data for the model calculations. The Fragmenting Particle model was chosen for these simulations as it best reflects the gasification behavior of the applied suspension fuel, as indicated by particle extraction experiments (see Appendix A.3 in supplementary material).

The experimentally observed longer flame in case of the suspension fuel is also predicted by the model, as shown by Fig. 1. The 2-Ph-FJM calculates a larger core zone at the nozzle exit than in the experiment. This effect is mainly caused by the description of the mixing in the near nozzle area in the 2-Ph-FJM as described in [18]. The longitudinal extension of the OH zone is slightly overestimated for MEG (ΔL_{OH} = 13%), whereas it is underpredicted for the suspension fuel (ΔL_{OH} = −19%). More details on model validation are given in supplementary material Appendix A.5.

Fig. 2(a) shows radial profiles of local mass based mixture fractions x_i of gasification agent (GA), syngas (SG), fuel vapor (FV) and gasified solid fuel (FG) at different nozzle distances for both cases calculated using the 2-Ph-FJM (see Eq. (4)). As described above, the entrainment of surrounding syngas is one decisive factor for the flame structure under EFG conditions. Because of the identical gas momentum flow, entrainment rates in both cases do not considerably differ, which is indicated by the similar values of x_{GA} and x_{SG}. However, it is evident that more liquid fuel evaporates in case of pure MEG than for the suspension fuel, as

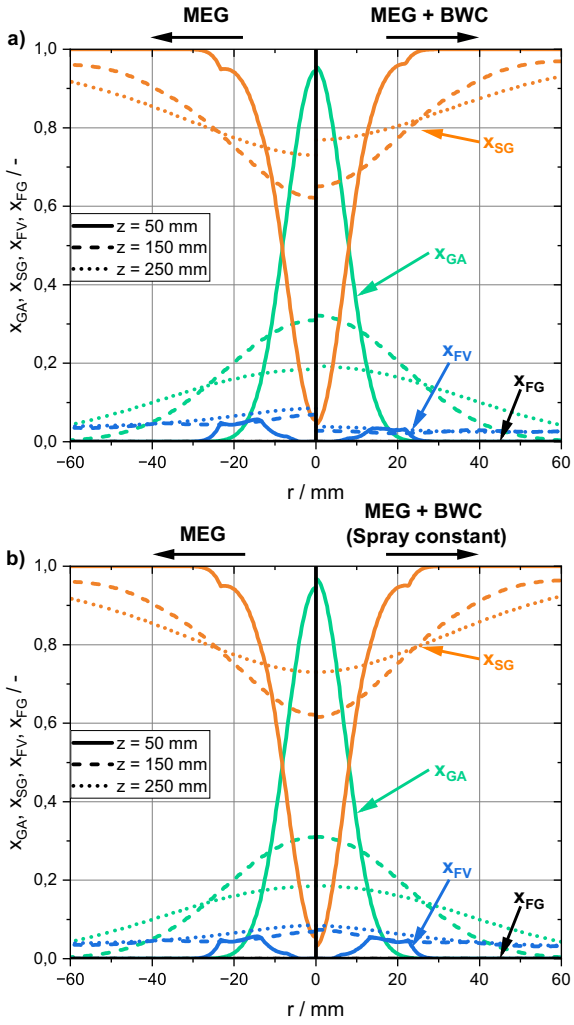

Fig. 2. Radial profiles of mass based mixture fractions of gasification agent (GA), syngas (SG), fuel vapor (FV) and gasified solid fuel (FG) for MEG and MEG + BWC calculated using the 2-Ph-FJM using the Fragmenting Particle model. a) shows results for the spray parameters given in Table 3, b) shows results where spray parameters of MEG were applied in both cases. Only the amount of liquid evaporation is significantly impacted, the entrainment of gas into the jet is not affected [18].

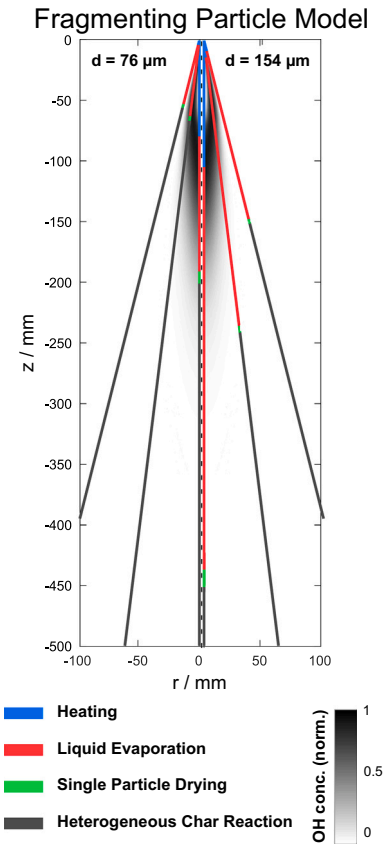

Fig. 3. Suspension droplet conversion steps along different model trajectories for two example droplet size classes with d = 75 µm and d = 154 µm from the droplet collective calculated using the 2-Ph-FJM. Input conditions of the suspension fuel case are applied. The respective OH distributions are shown in gray scale [18].

shown by the profiles of x_{FV}. The lower amount of liquid evaporation for the suspension fuel in comparison to MEG leads to a slower consumption of oxygen, causing a longer flame zone. This is reflected by the increase of L_{OH} = 197 mm (MEG, model) to 246 mm (MEG + BWC, model).

Fig. 2(b) shows that this effect is mostly caused by the influence of the spray parameters. Here, the original calculation for MEG is compared with a calculation for the suspension fuel, where input spray parameters of the MEG case were applied (see Table 3). The profiles of x_i in both cases are almost identical under the given conditions. The longitudinal extension of the OH zone shows similar values of L_{OH} = 197 mm (MEG) and 201 mm (MEG + BWC, spray parameters constant).

This indicates that the different liquid fuel evaporation rates caused by changes in spray parameters are mainly responsible for the observed enlargement of the OH zone when switching from liquid to suspension fuel. An additional factor could be inhibition of the evaporation rate with increasing solid content, which is not accounted for by the Fragmenting Particle model. This effect would further decrease evaporation rate and may explain the underprediction of L_{OH} for the suspension fuel in comparison to the experimental values. In all model calculations, gasified solid x_{FG} fuel is not present in significant amounts in the gas phase, implying that under the investigated conditions, solid reactions play a minor role in the processes in the burner near zone.

3.2. Comparison of suspension droplet models

In this section, the 2-Ph-FJM is applied to conduct a numerical study on the conversion of suspension droplets in the EFG flame and the impact of different droplet conversion models. Calculations are based on the input conditions of the suspension fuel case using spray parameters given in Table 3. First, the conversion steps of two droplet size classes d = 75 µm and d = 154 µm present in the investigated spray are analyzed in Fig. 3 for the Fragmenting Particle model. For each droplet size class, three different trajectories at angles of 0°, 7° and 15° from the jet centerline are examined. The modeled OH distribution in Fig. 3 is shown as a reference for the flame.

Starting from the nozzle exit, the graph shows an initial heating period, which is completed within short distance and within the OH zone for both droplet sizes. The following liquid evaporation step shows significant differences between both droplet size classes. Due to their lower mass, the 75 µm droplets require considerably less distance than the 154 µm droplets to complete the liquid evaporation step on all investigated trajectories. The droplets at the outer trajectories generally require a shorter nozzle distance to complete evaporation than the droplets at the jet centerline, which is caused by their lower velocities and thus longer residence times in comparison to the inner trajectories. When the solid volume fraction in a droplet increases during evaporation and the critical diameter is reached, the Fragmenting Particle model assumes the droplets disintegrate into single char particles surrounded by the remaining liquid. Due to the small diameter of the char particles, the following

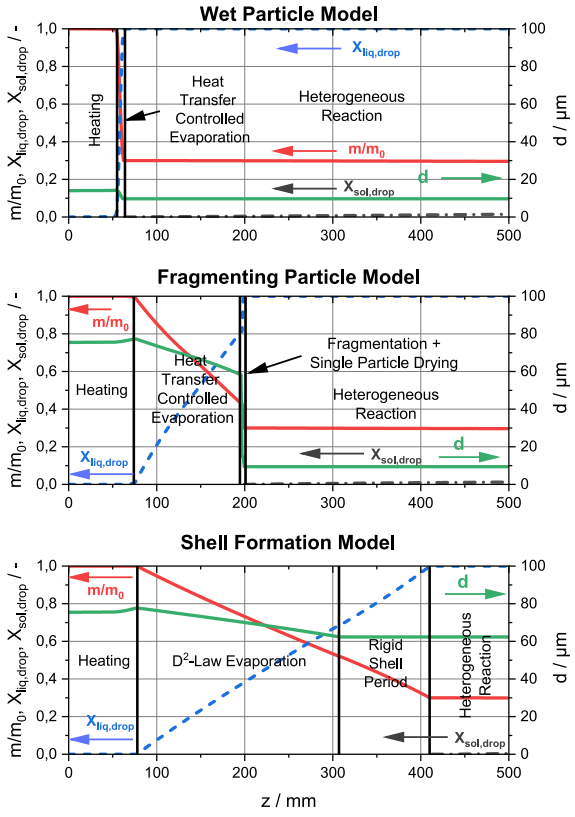

Fig. 4. Droplet mass, diameter, liquid evaporation progress and char conversion calculated for an individual 75 µm-droplet at a trajectory along the jet centerline using input data for case S30-A. The four droplet models investigated in this work are compared. Vertical lines indicate the droplet conversion regimes for each model [18].

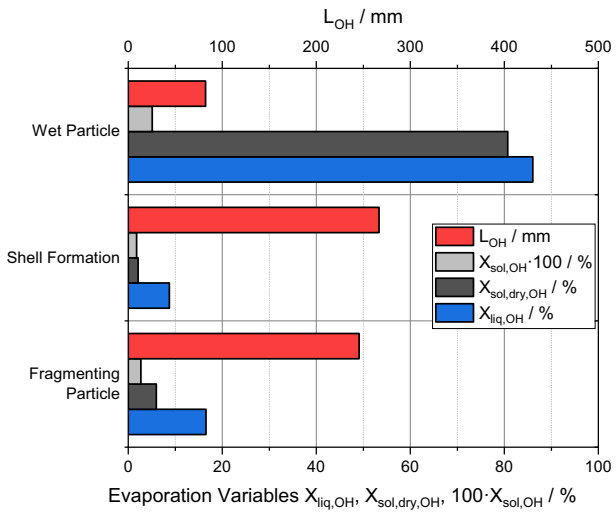

Fig. 5. Conversion progress variables and L_{OH} for the suspension fuel case compared for different suspension droplet models. The conversion progress variables are integrated over the entire spray within the boundaries of the OH volume. For visibility, the converted solid mass fraction is multiplied by a factor of 100 [18].

drying step is quick for both initial droplet sizes. Solid reactions then start when the remaining single particles have completely dried. The 75 µm droplets reach the solid conversion stage within or shortly after leaving the OH zone, while the 154 µm droplets only enter char conversion outside the OH boundaries. These results show that especially for the larger droplets, a significant amount of fuel vapor is released outside the OH zone. Char conversion is shown to predominantly take place outside the OH zone for both droplet size classes.

Fig. 4 shows a quantitative comparison of the three droplet models described in Sections 2.1.3 – 2.1.5. A 75 µm droplet on the jet centerline trajectory is selected as an example for the model comparison. Suspension droplet diameter d, evaporated liquid mass fraction $X_{\mathrm{liq,drop}}$, converted solid mass fraction $X_{\mathrm{sol,drop}}$ and normalized suspension droplet mass m/m_0 are displayed for each model.

The Wet Particle model assumes single char particles surrounded by a liquid film and thus derives the droplet size from the char particle diameter, liquid mass fraction and liquid density (Section 2.1.3). The diameter of all droplet classes using this model is thus set to 15 µm.

Fig. 4 shows that the initial droplet heat up period is similar for the investigated droplet models, with a shorter distance required to heat the droplets to the boiling for the Wet Particle Model, which is caused by the smaller initial droplet size.

In the following evaporation step, the low initial droplet diameter in case of the Wet Particle model causes an extremely short liquid evaporation distance of around $z = 62$ mm, where the liquid has completely evaporated and only solid phase is left. In the Fragmenting Particle model, the 75 µm droplet shrinks during evaporation until a critical droplet diameter is reached, which occurs at around $z = 200$ mm. At this point, the droplet disintegrates into individual char particles, each coated with a residual liquid film, analog to the Wet Particle model.

The fragmentation process substantially increases the surface area relative to the original suspension droplet, accelerating the evaporation rate and resulting in complete liquid evaporation at $z = 214$ mm.

In contrast, the Shell Formation model shows a significantly slower evaporation rate in comparison to the two models discussed above. The droplet first undergoes a receding diameter period up to the formation of a rigid porous shell, which is followed by a constant diameter period until the liquid has completely evaporated, leaving a spherical hollow agglomerate with a diameter of around $d = 62$ µm at $z = 419$ mm.

The solid conversion reactions start for all models when the liquid phase has completely evaporated. The devolatilization and heterogeneous gasification reactions are slow in comparison to the liquid evaporation processes. This is evident from the absence of notable mass reduction along the axial coordinate during this stage in all models. Since the solid phase leaves the flame zone in different conditions (single particle or agglomerate, as indicated by the droplet diameter), the conversion of the solid phase downstream of the flame in a technical gasifier is presumably strongly affected by these in-flame processes.

3.3. Impact of suspension droplet model on fuel conversion in flame

The results of the prior section showed major differences in liquid evaporation rates between the droplet models, suggesting a substantial influence of the droplet model on flame structure and fuel conversion variables. Fig. 5 shows the total evaporated mass fraction of liquid fuel $X_{\mathrm{liq,OH}}$, total mass fractions of dried char $X_{\mathrm{sol,dry,OH}}$ and converted char $X_{\mathrm{char,OH}}$ (for definitions see Section 2.1.2) integrated over all droplet size classes and the entire OH volume for input conditions and spray parameters of the suspension fuel case.

The Shell Formation model shows the lowest amount of liquid evaporation within the OH zone ($X_{\mathrm{liq,OH}} \approx 9\%$), while the Fragmenting Particle model predicts a higher amount of evaporation ($X_{\mathrm{liq,OH}} \approx 17\%$). The increased liquid evaporation for the Fragmenting Particle model decreases the longitudinal extension of the OH zone L_{OH} in comparison to the Shell Formation model. Both models produce L_{OH} values that are reasonable in comparison to the experimental value of $L_{OH} = 300$ mm. The Wet Particle model on the other hand produces high evaporation rates caused by the assumption of droplets being single solid particles coated in liquid, leading to around 86% fuel evaporation within the OH zone. The resulting longitudinal extension of the OH zone $L_{OH} = 82$ mm is however unrealistic.

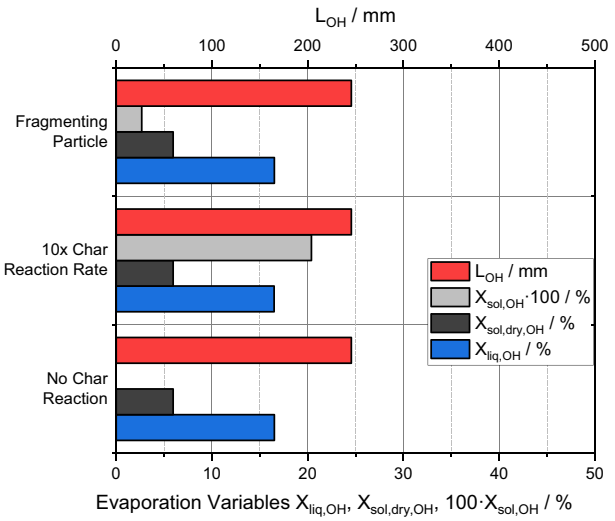

Fig. 6. Conversion progress variables and L_{OH} for the suspension fuel case compared for different modeling conditions using the Fragmenting Particle model as basis. The conversion progress variables are integrated over the entire spray within the boundaries of the OH volume. For better visibility, the converted solid mass fraction is multiplied by a factor of 100 [18].

Only few droplets completely dry up within the OH volume, as indicated by $X_{sol,dry,OH} \approx 2\%$ for the Shell Formation and $X_{sol,dry,OH} \approx 6\%$ for the Fragmenting Particle model. Due to the slow char gasification reactions, the total amount of char converted within the OH volume $X_{sol,OH}$ is significantly below 1% for all cases, even for the Wet Particle model.

The results show that the widely applied Wet Particle model approach is problematic due to the coupling of droplet and solid particle size, as this produces either unreasonable evaporation rates or incorrect solid particle sizes. The Fragmenting Particle approach showed plausible results for the applied reference fuel, but for more complex fuels undergoing pyrolysis reactions, a model considering shell formation should be applied to take the droplet conversion processes fully into account.

The impact of char reactions on the flame is further investigated using the Fragmenting Particle model. A calculation applying the basic char reaction rate is compared to a calculation featuring inert char particles and a calculation applying a char reaction rate increased by a factor of 10 (see Fig. 6). The comparison shows no significant impact of the char conversion rate on L_{OH}. The reason for this is that only a minor amount of char is released from the droplets within the OH zone as only the smallest droplets completely dry up within the flame (Fig. 3). The small amount of released char thus exhibits only a minor influence on local stoichiometry, which is further reduced by the slow reaction kinetics. As a consequence, the impact of the char particles on the flame can be considered limited in the investigated case. For the given conditions, the effect of the droplet model on the flame is thus mostly determined by its description of fuel evaporation.

For higher solid loadings, the amount and time of liquid evaporation are reduced and more solid fuel can be released from droplets within the flame. The devolatilization kinetics of the solid fuel gain relevance for the flame under such conditions and an impact on the flame can be expected. Especially for more reactive solid fuels, this effect would be more pronounced. In the boundary case of pure solid gasification, devolatilization overtakes the role of liquid evaporation and has been shown to influence the temperature field in a similar way for coal [32].

4. Conclusions

This work investigates the sub-processes during the conversion of suspension fuel droplets and their impact on the flame under conditions present in an Entrained Flow Gasifier (EFG) using modeling and experiments. A lack of experimentally validated model calculations for the flame zone of suspension fuel EFG was identified in literature, where most available studies apply simplified droplet models and do not assess suspension droplet conversion in the flame zone in detail. The differences between liquid and suspension fuel EFG flames have not been systematically investigated.

Within this scope, a numerical analysis is conducted applying a formerly developed 2-Phase Free Jet Model (2-Ph-FJM) that was expanded to describe the conversion of suspension fuel droplets. The model was validated in two EFG experiments using monoethylene glycol (MEG) and a reference suspension fuel consisting of MEG and beech-wood-char (BWC). OH concentrations calculated using the 2-Ph-FJM were compared to experimental OH-LIF data obtained at an atmospheric pressure EFG.

By comparison of the suspension fuel EFG flame structure to the liquid fuel EFG flame without solid particles, it was found that although the sub-processes in the flame become more complex, the reaction zone structure is not fundamentally changed when solid particles are added to the liquid fuel. It is shown that the entrainment of ambient syngas into the gas jet and the evaporation of liquid fuel are the decisive factors for the flame structure. The amount of solid particles released from droplets and the impact of solid reactions on the flame were low under the investigated conditions.

Concerning the conversion of the suspension droplets in the flame, a sensitivity analysis comparing the 3 different suspension droplet model approaches shows largely different rates of liquid evaporation, influencing flame structure. The results show that for an accurate description of the EFG flame for suspension fuels, special attention must be paid to the description of liquid evaporation during droplet conversion. This requires the selection of a suspension droplet conversion model appropriate to the applied fuel together with a correct droplet size and mass flux distribution. The widely applied Wet Particle approach is shown to be unsuitable due to the coupling of droplet and solid particle size, which produces either unrealistic evaporation rates or incorrect solid particle sizes. The Fragmenting Particle approach showed good results for the applied reference fuel. For more complex technical fuels undergoing pyrolysis reactions, a model considering shell formation should be applied. The 2-Ph-FJM demonstrates the ability to compare different droplet conversion models and to assess the impact of fuel properties on the EFG flame. This can serve as a basis for more complex CFD reactor simulations which are able to evaluate global reactor performance.

The results of this work emphasize that for the design of EFG systems for biomass and waste based suspension fuels, more work is needed to develop models that are able to predict the conversion of suspension droplets under EFG conditions. Especially the formation of solid agglomerates can impact global fuel conversion in technical gasifiers when suspension fuels are applied. It was also shown that for the fuel flexible operation of industrial gasifiers, special attention must be paid to the effect of solid particles on fuel rheology, which can impact atomization negatively. Larger droplets lead to a slower drying of the solid phase, increasing residence time required for fuel conversion. As further shown in this work, the increased droplet size for suspension fuels can influence temperature field in the reactor by inducing a longer flame zone in comparison to a liquid fuel. Research on the optimization of burners is needed.

CRediT authorship contribution statement

Manuel Haas: Writing – original draft, Visualization, Validation, Software, Methodology, Investigation, Formal analysis, Conceptualization. **Sabine Fleck:** Writing – review & editing, Supervision, Investigation. **Frederik Scheiff:** Writing – review & editing, Supervision. **Thomas Kolb:** Writing – review & editing, Supervision, Funding acquisition, Conceptualization.

Declaration of competing interest

The authors declare that they have no known competing financial interests or personal relationships that could have appeared to influence the work reported in this paper.

Acknowledgements

This work was supported by the Helmholtz Association of German Research Centers (HGF) in the context of the research program Materials and Technologies for the Energy Transition (MTET). The authors thank Tobias Jakobs (Karlsruhe Institute of Technology, Institute for Technical Chemistry, Gasification Technology) and Juliana Richter (Karlsruhe Institute of Technology, Institute for Technical Chemistry, Gasification Technology) for providing experimental facilities and support for the spray characterization experiments.

Appendix A. Supplementary data

Supplementary data for this article can be found online at doi:10.1016/j.fuel.2026.138473.

Data availability

Data will be made available on request.

References

[1] Eberhard M, Santo U, Michelfelder B, Günther A, Weigand P, Matthes J, Waibel P, Hagenmeyer V, Kolb T. The bioliq® Entrained–Flow Gasifier – a model for the German Energiewende. ChemBioEng Rev 2020;7(4):106–18.
[2] Voss R, Lee RP, Fröhling M. Chemical recycling of plastic waste: comparative evaluation of environmental and economic performances of gasification- and incineration-based treatment for lightweight packaging waste. Circ Econ Sustain 2022;2(4):1369–98.
[3] Ragaert K, Delva L, van Geem K. Mechanical and chemical recycling of solid plastic waste. Waste Manag(New York, N.Y.) 2017;69:24–58.
[4] Kusenberg M, Eschenbacher A, Djokic MR, Zayoud A, Ragaert K, de Meester S, van Geem KM. Opportunities and challenges for the application of post-consumer plastic waste pyrolysis oils as steam cracker feedstocks: to decontaminate or not to decontaminate? Waste management New York, N.Y. 2022;138:83–115.
[5] Broumand M, Albert-Green S, Yun S, Hong Z, Thomson MJ. Spray combustion of fast pyrolysis bio-oils: applications, challenges, and potential solutions. Prog Energy Combust Sci 2020;79:100834.
[6] Mularski J, Pawlak-Kruczek H, Modlinski N. A review of recent studies of the CFD modelling of coal gasification in entrained flow gasifiers, covering devolatilization, gas-phase reactions, surface reactions, models and kinetics. Fuel 2020;271:117620.
[7] Hasse C, Debiagi P, Wen X, Hildebrandt K, Vascellari M, Faravelli T. Advanced modeling approaches for CFD simulations of coal combustion and gasification. Prog Energy Combust Sci 2021;86:100938.
[8] Chen L, Yong SZ, Ghoniem AF. Oxy-fuel combustion of pulverized coal: characterization, fundamentals, stabilization and CFD modeling. Prog Energy Combust Sci 2012;38(2):156–214.
[9] Benyon PJ. Computational modeling of entrained flow slagging gasifiers [Ph.D. thesis]. Sydney: University of Sydney; 2002.
[10] Chen M-H, Chyou Y-P, Wang T. Simulation of coal gasification in a low-temperature, high-pressure entrained-bed reactor with a volatiles condensation and re-evaporation model. Appl Sci 2019;9(3):510.
[11] Handscomb CS, Kraft M, Bayly AE. A new model for the drying of droplets containing suspended solids. Chem Eng Sci 2009;64(4):628–37.
[12] Yao S-C, Liu L. Behavior of suspended coal-water slurry droplets in a combustion environment. Combust Flame 1983;51:335–45.
[13] Elperin T, Krasovitov B. Evaporation of liquid droplets containing small solid particles. Int J Heat Mass Transf 1995;38(12):2259–67.
[14] Roy Choudhury P. Slurry fuels. Prog Energy Combust Sci 1992;18(5):409–27.
[15] Holve DJ, Fletcher TH, Gomi K. Comparative combustion studies of ultrafine coal/water slurries and pulverized coal. Combust Sci Technol 1987;52(4–6):269–91.
[16] Haas M, Dammann M, Fleck S, Kolb T. Entrained flow gasification: impact of fuel spray distribution on reaction zone structure. Fuel 2023;334(4):126572.
[17] Bader A, Hartwich M, Richter A, Meyer B. Numerical and experimental study of heavy oil gasification in an entrained-flow reactor and the impact of the burner concept. Fuel Process Technol 2018;169:58–70.
[18] Haas M. Entrained flow gasification - conversion of liquid and suspension fuels in the burner near field. [Ph.D. thesis]., Karlsruhe: Karlsruhe Institute of Technology; 2026.
[19] Ahn KY, Baek SW, Choi CE. Investigation of a coal-water slurry droplet exposed to hot gas stream. Combust Sci Technol 1994;97(4–6):429–47.
[20] Vershinina KY, Glushkov DO, Kuznetsov GV, Strizhak PA. Differences in the ignition characteristics of coal–water slurries and composite liquid fuel. Solid Fuel Chem 2016;50(2):88–101.
[21] van Rossum G, Güell BM, Ramachandran RPB, Seshan K, Lefferts L, van Swaaij WPM, Kersten SRA. Evaporation of pyrolysis oil: product distribution and residue char analysis. AIChE J 2010;56(8):2200–10.
[22] Walsh PM, Zhang M, Farmayan WF, Beér JM. Ignition and combustion of coal-water slurry in a confined turbulent diffusion flame. Symp Int Combust 1985;20(1):1401–7.
[23] Murdoch PL, Pourkashanian M, Williams A. The mechanism of combustion of coal-water slurries. Symp Int Combust 1985;20(1):1409–18.
[24] Wong S-C, Lin A-C, Chi H-Y. Effects of surfactant on the evaporation, shell formation and disruptive behavior of slurry droplets. Symp Int Combust 1991;23(1):1391–7.
[25] Sitarski M. On the feasibility of secondary atomization of small slurry droplets exposed to intense thermal radiation. Combust Sci Technol 1987;54(1–6):177–201.
[26] Maloney DJ, Spann JF. Evaporation, agglomeration, and explosive boiling characteristics of coal-water fuels under intense heating conditions. Symp Int Combust 1989;22(1):1999–2008.
[27] Fradet Q. Novel modeling approaches for the entrained-flow gasification of bio-slurries. Dissertation, Universität Stuttgart; 2020.
[28] Hafner S. Modellentwicklung zur numerischen Simulation eines Flugstromvergasers für Biomasse. [Dissertation], Heidelberg: Ruprechts-Karls-Universität; 2010.
[29] Dammann M. Numerical modelling and simulation of atmospheric entrained flow gasification of surrogate fuels. Karlsruher Institut Für Technologie (KIT); 2024.
[30] Kim H-T, Lee J-H, Lee J-W, Lee B-H, Jeon C-H. Effect of operating conditions on the gasification of pet-coke water slurry in an entrained-flow gasifier simulation. ACS Omega 2023;8(48):45933–41.
[31] Nikrityuk PA, Meyer B. Gasification processes: modeling and simulation. John Wiley & Sons; 2014.
[32] Silaen A, Wang T. Effect of turbulence and devolatilization models on coal gasification simulation in an entrained-flow gasifier. Int J Heat Mass Transf 2010;53(9–10):2074–91.
[33] Luan Y-T, Chyou Y-P, Wang T. Numerical analysis of gasification performance via finite-rate model in a cross-type two-stage gasifier. Int J Heat Mass Transf 2013;57(2):558–66.
[34] Lan X, Zhong H, Gao J. CFD simulation on the gasification of asphalt water slurry in an entrained flow gasifier. Petroleum Sci 2014;11(2):308–17.
[35] Labbafan A, Ghassemi H. Numerical modeling of an E-Gas entrained flow gasifier to characterize a high-ash coal gasification. Energy Convers Manag 2016;112:337–49.
[36] Sun Z, Dai Z, Zhou Z, Guo Q, Yu G. Numerical simulation of industrial opposed multiburner coal–water slurry entrained flow gasifier. Ind Eng Chem Res 2012;51(6):2560–9.
[37] Choi YC, Li XY, Park TJ, Kim JH, Lee JG. Numerical study on the coal gasification characteristics in an entrained flow coal gasifier. Fuel 2001;80(15):2193–201.
[38] Xu J, Dai Z, Liu H, Guo L, Sun F. Modeling of multiphase reaction and slag flow in single-burner coal water slurry gasifier. Chem Eng Sci 2017;162(1):41–52.
[39] Fradet Q, Braun-Unkhoff M, Riedel U. A sectional approach for the entrained-flow gasification of slurry fuels. Energy Fuels 2018;32(12):12532–44.
[40] Lee A, Law CK. Gasification and shell characteristics in slurry droplet burning. Combust Flame 1991;85(1–2):77–93.
[41] Ashizawa M, Hara S, Kidoguchi K, Inumaru J. Gasification characteristics of extra-heavy oil in a research-scale gasifier. Energy 2005;30(11–12):2194–205.
[42] Stoesser P, Ruf J, Gupta R, Djordjevic N, Kolb T. Contribution to the understanding of secondary pyrolysis of biomass-based slurry under entrained-flow gasification conditions. Energy Fuels 2016;30(8):6448–57.
[43] Cheong HW, Jeffreys GV, Mumford CJ. A receding interface model for the drying of slurry droplets. AIChE J 1986;32(8):1334–46.
[44] Nešić S, Vodnik J. Kinetics of droplet evaporation. Chem Eng Sci 1991;46(2):527–37.
[45] Dalmaz N, Ozbelge HO, Eraslan AN, Uludag Y. Heat and mass transfer mechanisms in drying of a suspension droplet: a new computational model. Drying Technol 2007;25(2):391–400.
[46] Farid M. A new approach to modelling of single droplet drying. Chem Eng Sci 2003;58(13):2985–93.
[47] Moszkowicz P, Witzel L, Claus G. Modelling of very fast pyrolysis of heavy fuel oil droplets. Chem Eng Sci 1996;51(17):4075–86.
[48] Hallett WLH, Clark NA. A model for the evaporation of biomass pyrolysis oil droplets. Fuel 2006;85(4):532–44.
[49] Ganji MJZ, Ghassemi H. Theoretical shell formation model for single droplet of heavy fuel oil. J Anal Appl Pyrolysis 2023;169(5):105760.
[50] Hotz C, Haas M, Wachter S, Fleck S, Kolb T. Two-phase free jet model of an atmospheric entrained flow gasifier. Fuel 2021;304(21–23):121392.
[51] Hunger F, Stelzner B, Trimis D, Hasse C. Flamelet-Modeling of inverse rich diffusion flames. Flow Turbulence Combust 2013;90(4):833–57.
[52] McBride BJ. NASA glenn coefficients for calculating thermodynamic properties of individual species. National Aeronautics and Space Administration, John H. Glenn Research Center; 2002.
[53] Verein Deutscher Ingenieure. VDI-wärmeatlas. 11 ed. Berlin, Heidelberg: Springer Berlin Heidelberg; 2013.

[54] Dammann M, Walker SC, Mancini M, Kolb T. Devolatilisation of beech wood char: kinetics from thermogravimetric analyses and drop-tube reactor experiments. Fuel 2024;375:131967.
[55] Kreitzberg T, Phounglamcheik A, Haugen NEL, Kneer R, Umeki K. A shortcut method to predict particle size changes during char combustion and gasification under regime II conditions. Combust Sci Technol 2022;194(2):272–91.
[56] Schneider C, Zeller M, Böhm D, Kolb T. Influence of pressure on the gasification kinetics of two high-temperature beech wood chars with CO2, H_2O and its mixture. Fuel 2021;299:120523.
[57] Fleck S, Santo U, Hotz C, Jakobs T, Eckel G, Mancini M, Weber R, Kolb T. Entrained flow gasification. Part 1: Gasification of glycol in an atmospheric-pressure experimental rig. Fuel Apr 2018;217:306–19.